Journal of Computational Applied Mechanics 2026, 57(4): 554-568

DOI: 10.22059/jcamech.2026.417757.1872

RESEARCH PAPER

Pulsatile Nanofluid Flow and Nanoparticle Transport in a Stenosed Bifurcated Artery

Zeshan Pervaiz [a], Obaid Ullah Mehmood [b], Ahmed Zeeshan [a, c,*], Arshad Riaz [d], Islom Kadiov [e]

[a] Department of Mathematics & Statistics, Faculty of Science, International Islamic University, Islamabad, 44000, Pakistan

[b] Department of Mathematics, COMSATS University Islamabad, Wah Campus, Islamabad, 47040, Pakistan
[c] Department of Mathematics, College of Science, Korea University, 145 Anam-ro, Seongbuk-gu, Seoul 02841, Republic of Korea
[d] Department of Mathematics, University of Education, Jauharabad Campus, Pakistan
[e] Department of Mathematics, Urgench State University, Uzbekistan

Abstract

This work presents an analytical model for pulsatile nanofluid flow and coupled heat-mass transport in a stenosed bifurcated artery. Flow is modeled as an incompressible laminar nanofluid, and the governing continuity, momentum, energy and concentration equations are formulated in cylindrical coordinates with stenosis on the outer wall of the parent branch. A radial coordinate transformation consistent with the nonuniform arterial radius is employed to derive modified forms of the energy and concentration equationsalong with thermophoresis (Soret effect) and curvature induced spatial gradients are retained. After nondimensionalization, the resulting system for axial velocity, temperature and concentration in the parent and daughter branches is solved under physiological boundary conditions, and the influence of key dimensionless groups is examined parametrically. The results show that increasing nanoparticle volume fraction, thermal expansion coefficient, Grashof number, Brownian motion parameter and Soret number enhances axial velocity and elevates core temperature in both parent and daughter segments, while higher Lewis number reduces both temperature and concentration fields, due to diffusive damping mechanism. Lewis numbers, indicating intensified nanoparticle dispersion, whereas the daughter branches exhibit non-monotonic concentration behavior that reflects the competing roles of geometry and thermo diffusion in downstream nanoparticle delivery. These findings provide a mechanistic basis for optimizing nanoparticle assisted drug delivery and thermal therapies in stenosed bifurcated arterial networks.

Keywords: Nanofluid; Bifurcated geometry; Stenosed channel; Brownian motion; Thermophoresis; Soret effect;

1. Introduction

Nanofluids are engineered colloidal suspensions of nanoparticles dispersed in base fluids such as water, ethylene glycol, or biological fluids like blood. The concept of nanofluids was first introduced by [1]who showed that

* Corresponding author.
E-mail address: ahmedzeeshan@korea.ac.kr

nanoparticles significantly enhance the thermal conductivity and heat transfer capability of conventional fluids. Later, [2] proposed a widely used single-phase nanofluid model that incorporates nanoparticle volume fraction directly into the governing equations, simplifying the analysis of nanofluid transport. [3] further improved nanofluid modeling by introducing a two-component approach that considers Brownian motion and thermophoresis as the primary mechanisms responsible for nanoparticle transport.

Nanofluids have attracted considerable attention in biomedical applications, particularly for modeling nanoparticle transport in blood flow systems. [4] investigated nanofluid flow in arteries and showed that nanoparticles influence both flow resistance and heat transfer behavior. [5] studied nanofluid transport in curved channels and demonstrated the importance of curvature in biofluid flow. [6] analyzed nanofluid heat transfer in complex geometries and reported enhanced thermal performance due to nanoparticle addition. [7]examined different nanofluid models and highlighted the influence of nanoparticle concentration on thermal characteristics. [8] studied boundary layer nanofluid flow and emphasized the role of thermophysical properties in controlling heat transfer processes. [9] investigated magnetohydrodynamic nanofluid flow and showed that magnetic fields can influence nanoparticle transport.

Bifurcated arterial geometries play an important role in understanding complex blood flow behavior in the human vascular system. [10] first identified the relationship between wall shear stress and atherosclerosis development in arterial bifurcations. [11] further investigated pulsatile flow in carotid bifurcations and demonstrated the role of disturbed flow patterns in disease formation. [12] developed computational models for blood flow in vascular networks. [13] applied finite element methods to simulate arterial hemodynamics in realistic geometries. [14] experimentally studied flow through stenosed arteries and observed recirculation zones and flow separation. [15] used particle image velocimetry techniques to analyze velocity fields in bifurcation models.

Further studies incorporated realistic rheological properties of blood in bifurcated arteries. [16] performed computational simulations of non-Newtonian blood flow in carotid artery bifurcations. [17]also investigated non-Newtonian blood flow in symmetric bifurcated arteries and demonstrated its effect on velocity and shear stress distributions. More recently, researchers have incorporated nanofluid transport mechanisms in vascular systems. [18] studied nanofluid heat transfer under external forces and thermal effects. [19] analyzed nanofluid transport in biological flows and demonstrated the combined influence of magnetic fields and nanoparticles. [20] investigated pulsatile nanofluid flow in stenosed bifurcated arteries and highlighted the effects of nanoparticle volume fraction, Brownian motion, and thermophoresis on velocity, temperature, and concentration distributions.

In this research, a concentration equation of a nanoparticle in a bifurcated artery is modified in order to offer nanofluid flow. The formulation of nanoparticle transport considers the effects of curvature and branching (in contrast to more traditional straight-vessel models) to determine the transport of nanoparticles. The model consists of Brownian diffusion and thermophoresis and a radial transformation and concentration gradient across the bifurcated branches is captured.

The realistic boundary conditions of the parent artery and the daughter artery are also used to study the effects of asymmetric daughter branches. Such a method enhances insight into the nanoparticle distribution in complicated vascular geometries, which is significant in targeted drug delivery and biomedical nanofluid.

Nanofluids suspension of nanoparticles in base fluids, e.g. blood, increases the rate of heat and mass transfer and has found extensive medical applications, such as cancer therapy and vascular diagnostics. Because bifurcation of arteries is a natural process, at which flow becomes nonlinear with separation and recirculation, the geometries of these bifurcated arteries will give a more realistic understanding of nanoparticle transport compared to a straight-vessel model.

2. Problem Formulation

In this context, the present work investigates the flow of nanofluid through a bifurcated arterial geometry, considering blood as the base fluid. The governing equations including continuity, momentum, and energy equations are employed under laminar, incompressible, and steady-state assumptions. A particular novelty of this study lies in the formulation and analysis of a new concentration equation for nanoparticle transport, tailored to reflect the geometrical complexity and physiological conditions at bifurcations.

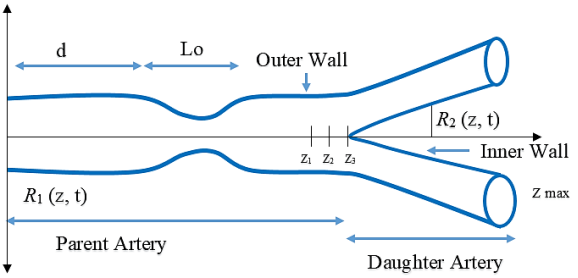

Figure 1: Geometry of the problem

2.1. Geometry Description

Figure 1 illustrates the geometry of the problem. The bifurcated artery walls having time-dependent stenosis on the outer wall in mathematical form is represented by R_1 whereas inner wall is represented by R_2 and is defined below:

$$R_1(z,t)=\begin{cases} R_0\Omega(t), & 0\le z\le d \\ \left(R_0-\dfrac{4\delta}{l_0^2}\left(l_0(z-d)-(z-d)^2\right)\right)\Omega(t), & d\le z\le d+L_0 \\ R_0\Omega(t), & d+L_0\le z\le z_1 \\ \left(R_0-r_0-\sqrt{\left(r_0^2-(z-z_1)^2\right)}\right)\Omega(t), & z_1\le z\le z_2 \\ \left(2r_1\sec\alpha+(z-z_2)\tan\alpha\right)\Omega(t), & z_2\le z\le z_{\max} \end{cases} \tag{1}$$

Where, $\Omega(t)$ is described as $\Omega(t)=1-e^{-\lambda\omega t}\left(\cos\omega t-1\right)\lambda$.

$$R_2(z,t)=\begin{cases} 0, & 0\le z\le z_3 \\ \sqrt{\left(r_0'^2-\left(z-z_3-r_0'\right)^2\right)}, & z_3\le z\le z_3+r_0'(1-\sin\alpha) \\ (z-z_2)\tan\alpha, & z_3+r_0'(1-\sin\alpha)\le z\le z_{\max} \end{cases} \tag{2}$$

The curvature of lateral junction is represented by r_0 and is described below:

$$r_0=\frac{1-2r_1\sec\alpha}{\cos\alpha-1} \tag{3}$$

The curvature of the flow divider is represented by r_0' and is described as:

$$r_0'=\frac{(z_3-z_2)\sin\alpha}{1-\sin\alpha},\quad z_2=z_1+r_0\sin\alpha,\quad z_3=z_2+q_1. \tag{4}$$

2.2. Governing Equations

The concentration equation incorporates the effects of Brownian motion, thermophoresis, and spatial transformation using a radial coordinate transformation, which aligns the model with variable arterial wall geometry. Moreover, distinct boundary conditions are imposed at the parent and daughter branches to more accurately represent real physiological flow behaviour. This approach provides a more comprehensive and realistic insight into nanoparticle distribution, which is essential for evaluating drug targeting efficiency and thermal behaviour in

branching blood vessels.

Basic equations describing the fluid flow are:

Continuity:

$$\frac{\partial V_r}{\partial r}+\frac{V_r}{r}+\frac{\partial V_z}{\partial z}=0 \tag{5}$$

Momentum (r-component):

$$\rho_{nf}\left(\frac{\partial V_r}{\partial t}+V_r\frac{\partial V_r}{\partial r}+V_z\frac{\partial V_r}{\partial z}\right)=-\frac{\partial p}{\partial r}+\mu_{nf}\left(\frac{\partial^2 V_r}{\partial r^2}+\frac{1}{r}\frac{\partial V_r}{\partial r}-\frac{V_r}{r^2}+\frac{\partial^2 V_r}{\partial z^2}\right) \tag{6}$$

Momentum (z-component):

$$\rho_{nf}\left(\frac{\partial V_z}{\partial t}+V_r\frac{\partial V_z}{\partial r}+V_z\frac{\partial V_z}{\partial z}\right)=-\frac{\partial p}{\partial z}+\mu_{nf}\left(\frac{\partial^2 V_z}{\partial r^2}+\frac{1}{r}\frac{\partial V_z}{\partial r}+\frac{\partial^2 V_z}{\partial z^2}\right)+(1-\phi)\rho_f g\beta_f(T-T_0) \tag{7}$$

Energy:

$$(\rho c_p)_{nf}\left(\frac{\partial T}{\partial t}+V_r\frac{\partial T}{\partial r}+V_z\frac{\partial T}{\partial z}\right)=k_{nf}\left(\frac{\partial^2 T}{\partial r^2}+\frac{1}{r}\frac{\partial T}{\partial r}+\frac{\partial^2 T}{\partial z^2}\right)+D_T\left(\frac{\partial^2 C}{\partial r^2}+\frac{\partial^2 C}{\partial z^2}\right)+Q(T-T_0) \tag{8}$$

Concentration:

$$\frac{\partial C}{\partial t}+V_r\frac{\partial C}{\partial r}+V_z\frac{\partial C}{\partial z}=D_S\left(\frac{\partial^2 C}{\partial r^2}+\frac{1}{r}\frac{\partial C}{\partial r}+\frac{\partial^2 C}{\partial z^2}\right)+\frac{D_C}{T_0}\left(\frac{\partial^2 T}{\partial r^2}+\frac{1}{r}\frac{\partial T}{\partial r}+\frac{\partial^2 T}{\partial z^2}\right) \tag{9}$$

2.3. Boundary Conditions

The appropriate boundary conditions are:

$$\frac{\partial V_z}{\partial r}=0,\ \frac{\partial T}{\partial r}=0,\ \frac{\partial C}{\partial r}=0,\ \text{at } r=0,\ \text{for } 0\le z\le z_3 \tag{10}$$

$$V_z=0,\ T=T_0,\ C=C_0,\ \text{at } r=R_1(z,t)\ \text{for all } z \tag{11}$$

$$V_z=0,\ T=T_1,\ C=C_1,\ \text{at } r=0\ \text{for } z_3\le z\le z_\infty. \tag{12}$$

2.4. Nanofluid Properties

The viscosity of nanofluid model is represented by [1], [2]:

$$\mu_{nf}=\frac{\mu_f}{(1-\phi)^{2.5}},\ \rho_{nf}=(1-\phi)\rho_f+\phi\rho_s,\ (c_p)_{nf}=(c_p)_s\phi+(1-\phi)(c_p)_f$$
$$(\rho\beta)_{nf}=(1-\phi)(\rho\beta)_f+\phi(\rho\beta)_s,\ k_{nf}=\frac{k_s+2k_f-2\phi(k_f-k_s)}{k_s+2k_f+\phi(k_f-k_s)}k_f \tag{13}$$

Where μ_f is viscosity of fluid and ϕ is the nanofluid volume fraction. ρ_f is density of fluid, ρ_s shows density of nanoparticles. $(\rho c_p)_f$ is a heat capacitance of fluid, $(\rho c_p)_s$ heat capacitance of nanoparticles. k_f is thermal conductivity of fluid, k_s is thermal conductivity of nanoparticles. Where k_{nf} and $(\rho c_p)_{nf}$ are thermal

conductivity and heat capacitance of nanofluid model. $(\rho\gamma)_f$ represents density and thermal expansion coefficient of fluid, $(\rho\gamma)_s$ represents density and thermal expansion coefficient of nanoparticles.

Thermo-physical Properties	Blood	Copper
c_p (J/kg·K)	3594	385
ρ (kg/m³)	1063	8933
k (W/m·K)	0.492	400
β (10^{-5} 1/K)	0.18	1.67

Table 1: Thermo-physical parameters for blood and copper

3. Dimensionless Formulation

3.1. Dimensionless Variables

Utilizing the dimensionless quantities:

$$r^* = \frac{r}{R_0}, z^* = \frac{z}{L_0}, V_r^* = \frac{V_r L_0}{u_0}, V_z^* = \frac{V_z}{u_0}, \theta = \frac{T - T_0}{T_1 - T_0}, \Phi = \frac{C - C_0}{C_1 - C_0},$$
$$t^* = \frac{u_0 t}{L_0}, P^* = \frac{P}{\rho_{nf} u_0^2}, Q_0 = \frac{T_1 - T_0}{\rho_{nf} u_0^2}, k = \frac{c_p \mathrm{Re} \rho_{nf} u_0 R_0}{\mu_{nf}},$$
$$Gr = \frac{g(1-\phi)\beta_f (T_1 - T_0) R_0^3}{\rho_{nf} u_0}, Pr = \frac{\mu_{nf}}{\rho_{nf} \alpha_{nf}}, Le = \frac{\alpha_{nf}}{D_S}, \quad (14)$$
$$Nb = \frac{D_T (C_1 - C_0)}{\alpha_{nf}}, Sr = \frac{D_C T_0 (T_1 - T_0)}{D_S (C_1 - C_0)}.$$

3.2. Dimensionless Governing Equations

Equations (5) to (9) become (dropping asterisks for convenience):

Continuity:

$$\frac{\partial V_r}{\partial r} + \frac{V_r}{r} + \frac{\partial V_z}{\partial z} = 0. \quad (15)$$

Momentum (r-component):

$$\mathrm{Re}\delta^3 \left(\frac{\partial V_r}{\partial t} + V_z \frac{\partial V_r}{\partial z} + V_r \frac{\partial V_r}{\partial r} \right) = -\frac{\partial p}{\partial r} + \delta^2 \left(\frac{\partial^2 V_r}{\partial r^2} + \frac{1}{r}\frac{\partial V_r}{\partial r} + \delta^2 \frac{\partial^2 V_r}{\partial z^2} - \frac{V_r}{r^2} \right). \quad (16)$$

Momentum (z-component):

$$\mathrm{Re} \left(\frac{\partial V_z}{\partial z} + V_z \frac{\partial V_z}{\partial z} + V_r \frac{\partial V_z}{\partial r} \right) = -\frac{\partial p}{\partial z} + \left(\frac{\partial^2 V_z}{\partial r^2} + \frac{1}{r}\frac{\partial V_z}{\partial r} + \delta^2 \frac{\partial^2 V_z}{\partial z^2} \right) + Gr\theta \quad (17)$$

.

Energy:

$$Pr\,\mathrm{Re}\left(\frac{\partial\theta}{\partial t}+V_z\frac{\partial\theta}{\partial z}+V_r\frac{\partial\theta}{\partial r}\right)=\delta^2\left(\frac{\partial^2\theta}{\partial r^2}+\frac{1}{r}\frac{\partial\theta}{\partial r}+\delta^2\frac{\partial^2\theta}{\partial z^2}\right)+Nb\left(\frac{\partial^2\Phi}{\partial r^2}+\frac{1}{r}\frac{\partial\Phi}{\partial r}\right). \tag{18}$$

Concentration:

$$Pr\,\mathrm{Re}\left(\frac{\partial\Phi}{\partial t}+V_r\frac{\partial\Phi}{\partial r}+V_z\frac{\partial\Phi}{\partial z}\right)=\frac{1}{Le}\left(\frac{\partial^2\Phi}{\partial r^2}+\frac{1}{r}\frac{\partial\Phi}{\partial r}+\delta^2\frac{\partial^2\Phi}{\partial z^2}\right)+Sr\left(\frac{\partial^2\theta}{\partial r^2}+\frac{1}{r}\frac{\partial\theta}{\partial r}+\delta^2\frac{\partial^2\theta}{\partial z^2}\right). \tag{19}$$

3.3. Mild Stenosis Approximation

After removing dashes and applying mild stenosis approximation ($\delta \ll 1$), equations (15) to (19) become:

$$\frac{\partial P}{\partial r}=0, \tag{20}$$

$$\frac{\partial P}{\partial z}=s\left(\frac{\partial^2 V_z}{\partial r^2}+\frac{1}{r}\frac{\partial V_z}{\partial r}\right)+G_r\theta, \tag{21}$$

$$\frac{\partial^2\theta}{\partial r^2}+\frac{1}{r}\frac{\partial\theta}{\partial r}+N_c\left(\frac{\partial^2 C}{\partial r^2}+\frac{1}{r}\frac{\partial C}{\partial r}\right)+\beta\theta=0, \tag{22}$$

$$L_e\left(\frac{\partial^2 C}{\partial r^2}+\frac{1}{r}\frac{\partial C}{\partial r}\right)+S_r\left(\frac{\partial^2\theta}{\partial r^2}+\frac{1}{r}\frac{\partial\theta}{\partial r}\right)=0, \tag{23}$$

The pressure gradient $\frac{\partial P}{\partial z}=A_0+A_1 cos\omega t$, where $\omega=2\pi f$, f is the pulse frequency, A_0 and A_1 are pressure gradient of steady flow and amplitude of oscillatory part, and t is time. Which is taken as P.

3.4. Radial Transformation

$\xi=\frac{r-R_2}{R}$, where $R=R_1-R_2$, (24)

Utilizing the radial transformation, equations (21) to (23) become:

$$\frac{1}{(1-\phi)^{2.5}}\left(\frac{1}{R^2}\frac{\partial^2 V_z}{\partial\xi^2}+\frac{1}{R(\xi R+R_2)}\frac{\partial V_z}{\partial\xi}\right)+\frac{(\rho\gamma)_{nf}}{(\rho\gamma)_n}G_r\theta-P=0, \tag{25}$$

$$\frac{1}{R^2}\frac{\partial^2\theta}{\partial\xi^2}+\frac{1}{R(\xi R+R_2)}\frac{\partial\theta}{\partial\xi}+N_c\left(\frac{1}{R^2}\frac{\partial^2 C}{\partial\xi^2}+\frac{1}{R(\xi R+R_2)}\frac{\partial C}{\partial\xi}\right)+\frac{2k_f+k_s-2\phi\left(k_f-k_s\right)}{2k_f+k_s+2\phi\left(k_f-k_s\right)}\beta=0, \tag{26}$$

$$L_e\left(\frac{1}{R^2}\frac{\partial^2 C}{\partial\xi^2}+\frac{1}{R(\xi R+R_2)}\frac{\partial C}{\partial\xi}\right)+S_r\left(\frac{1}{R^2}\frac{\partial^2\theta}{\partial\xi^2}+\frac{1}{R(\xi R+R_2)}\frac{\partial\theta}{\partial\xi}\right)=0, \tag{27}$$

Subject to the boundary conditions:

$$\frac{\partial V_z}{\partial\xi}=0,\quad \frac{\partial\theta}{\partial\xi}=0,\quad \frac{\partial C}{\partial\xi}=0,\quad at\ \xi=0,\quad for\quad 0\le z\le z_3 \tag{28}$$

$$V_z=0,\quad \theta=0,\quad C=0\quad at\ \xi=1,\quad for\ all\quad z \tag{29}$$

$$V_z=0,\quad \theta=1,\quad C=1\quad at\ \xi=0\quad for\quad z_3\le z\le z_{max} \tag{30}$$

4. Solution Method

Equations (25) to (27) are solved exactly using the boundary conditions given in equations (28) to (30). The obtained solutions for velocity, temperature, and concentration are analyzed in two cases.

Case 1: Parent Artery- This case considers the region $\left(R_0-\frac{4\delta}{l_0^2}\left(l_0(z-d)-(z-d)^2\right)\right)\Omega(t)$ for $0 \le z \le z_3$. Which represents the stenotic region.

Case 2: Daughter Artery- This case we consider $\left(2r_1\sec\alpha+(z-z_2)\tan\alpha\right)\Omega(t)$ for $z_3 \le z \le z_{max}$. It represents the daughter artery.

.

5. Results and Discussion

The results are illustrated through computationally obtained graphs in this section. These graphs provide a comprehensive overview of velocity, temperature and concentration profiles under the influence of various parameters affecting the flow of a non-Newtonian fluid. Mathematica is utilized to evaluate and predict velocity, temperature and concentration profile and the effects of various parameters. Several key aspects are discussed to better understand and facilitate blood flow through the stenotic artery, which consists of both parent and daughter branches. The graphs are plotted using fixed values such as d=4, δ =0.45, q_1 =0.45, r_1 =0.60, and an angle of π/6 as discussed below.

5.1. Case 1: Parent Artery

5.1.1. Parental Velocity Profile

Figure 2(a): This graph shows that as the nanoparticle volume fraction ϕ increases from 0.01 to 0.04, the velocity profile Vp enhances across the channel. The presence of more nanoparticles increases the thermal conductivity of the fluid, which reduces the fluid's viscosity and promotes better flow. The peak velocity becomes more pronounced with higher ϕ, indicating stronger nanofluid effects. Figure 2(b): An increase in β (from 0.11 to 0.14) results in a noticeable rise in Vp. This behaviour is attributed to enhanced buoyancy forces due to stronger thermal gradients, which accelerate the fluid flow in the parent channel. The peak of the velocity curve shifts upward with increasing β, confirming the thermally-driven flow augmentation. Figure 2(c): As the Grashof number increases (from 0.0030 to 0.0034), the velocity increases as well. This is consistent with the fact that *Gr* represents the ratio of buoyancy to viscous forces. Higher values imply stronger buoyancy-driven flow, leading to improved circulation and higher axial velocity in the parent branch. Figure 2(d): With increasing *Nb* (from 0.1 to 0.4), the velocity profile shifts upward. Brownian motion enhances the diffusion of nanoparticles, which in turn affects the energy and momentum transfer in the flow. The result is an increased velocity due to more efficient distribution of heat and mass within the fluid. Figure 2(e): An inverse effect is observed with increasing *Le* (from 1 to 4). The Lewis number indicates the ratio of thermal to mass diffusivity. Higher values mean reduced nanoparticle diffusion, which suppresses the overall velocity. This suggests that mass transport becomes limited at higher *Le*, reducing momentum transfer in the parent artery. Figure 2(f): Velocity increases with higher values of the Soret number (from 0.10 to 0.70). The Soret effect introduces thermophoretic migration of nanoparticles from hot to cold regions. This additional mass flux reinforces the flow dynamics, leading to a steeper velocity profile in the center of the channel.

5.1.2. Parental Temperature Profile

Figure 3(a): As ϕ increases from 0.01 to 0.04, the temperature θp within the parent channel rises. This is because a higher volume fraction of nanoparticles enhances the effective thermal conductivity of the base fluid. Consequently, more heat is retained and distributed across the flow, leading to a higher thermal boundary layer thickness and elevated temperature profiles. Figure 3(b): An increase in β (from 0.11 to 0.14) causes a noticeable rise in temperature. A larger β amplifies the buoyancy-driven thermal forces, which promote enhanced convective transport. This leads to a stronger thermal gradient and elevates the core fluid temperature. The parabolic shape also becomes sharper near the center, indicating more localized heat retention. Figure 3(c): With increasing *Sr* from 0.10

to 0.70, the temperature field becomes more pronounced. The Soret effect or thermal diffusion leads to the migration of nanoparticles from hot to cold regions, and this redistribution enhances energy transport.

Parental Velocity

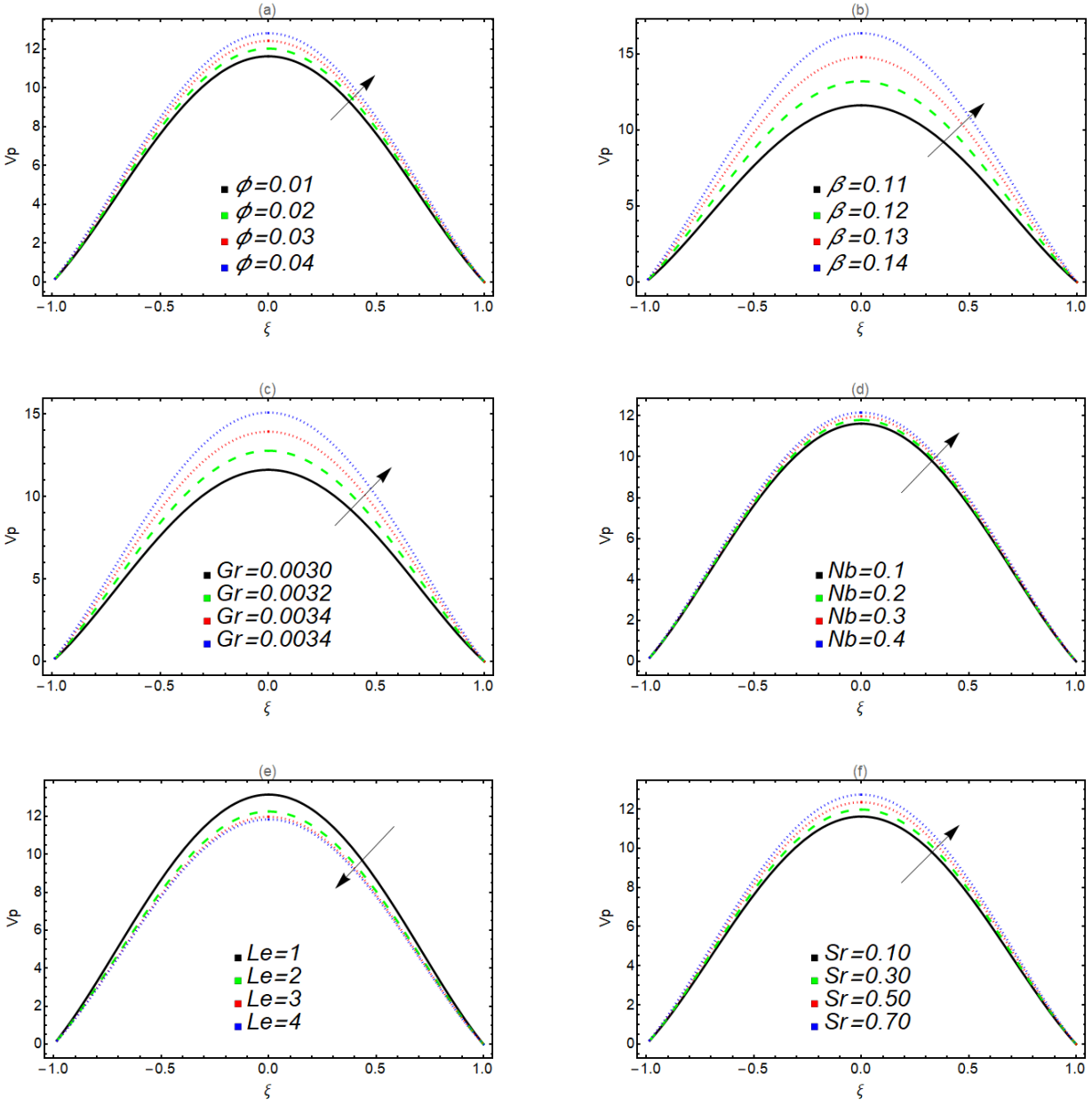

Figure 2: Parental Velocity Profile Vp on different variations of nanoparticle volume fraction ϕ, Brownian motion parameter *Nb*, Soret number *Sr*, and Lewis number *Le*, Thermal Expansion Coefficient β, Grashof Number *Gr*.

Parental Temperature

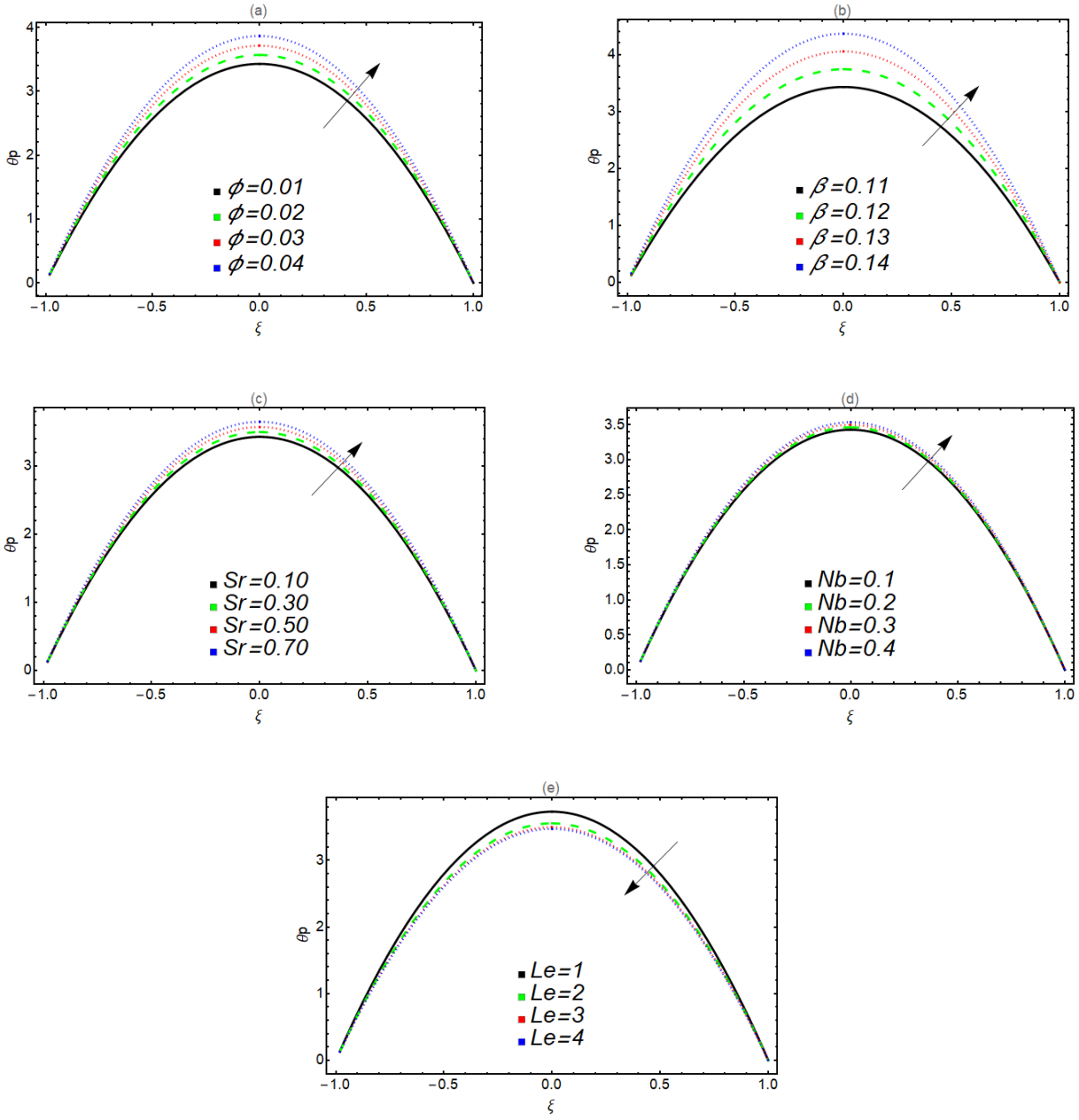

Figure 3: Parental Temperature Profile θp on different variations of nanoparticle volume fraction ϕ, Brownian motion parameter *Nb*, Soret number *Sr*, and Lewis number *Le*, Thermal Expansion Coefficient β.

As a result, the central peak in θp rises, indicating stronger thermophoretic effects in nanofluids under bifurcated flow. Figure 3(d): As *Nb* increases from 0.1 to 0.4, the parental temperature also increases slightly. This is because Brownian motion boosts random nanoparticle motion, enhancing energy exchange between particles and the fluid. This effect improves thermal conductivity and leads to a marginal rise in temperature. The influence is less sharp compared to ϕ and *Sr*, indicating a milder thermal impact of Brownian diffusion. Figure 3(e): Here, increasing *Le* from 1 to 4 leads to a reduction in temperature distribution. The Lewis number represents the ratio of thermal diffusivity to mass diffusivity, and higher values imply reduced nanoparticle diffusion. This decrease in nanoparticle movement dampens the convective heat transfer process, lowering θp. Hence, *Le* acts as a cooling or resistance factor in thermal transport.

5.1.3. Parental Concentration Profile

Figure 4(a): As the nanoparticle volume fraction ϕ increases from 0.01 to 0.04, the concentration profiles show a slight decrease in magnitude across the cross-section. This is due to the enhanced interaction between nanoparticles and the base fluid, which leads to a more uniform distribution of concentration. The profiles are symmetric about ξ=0, confirming the geometrical symmetry of the bifurcated channel. Figure 4(b): Increasing the bifurcation angle β from 0.11 to 0.14 leads to a noticeable decrease in concentration magnitude. A larger bifurcation angle modifies the geometry, effectively redistributing the concentration field. This geometrical expansion influences the local mass diffusion, showing that concentration becomes more diluted in the wider channel. Figure 4(c): The Soret effect plays a significant role here: with increasing *Sr* from 0.10 to 0.70, the concentration profile becomes increasingly negative in magnitude. This suggests that stronger thermal diffusion (thermodiffusion) drives nanoparticles more aggressively from hot to cold regions, causing steeper concentration gradients. The profiles steepen symmetrically due to equal thermophoretic pull in both channel halves. Figure 4(d): An increase in *Nb* from 0.1 to 0.4 shows a slight decrease in concentration magnitude. This is because greater Brownian motion promotes enhanced random movement of nanoparticles, tending toward a more homogeneous distribution and thus reducing net concentration gradients. The small variation indicates a subtle role of Brownian diffusion compared to Soret effects. Figure 4(e): As *Le* increases from 1 to 4, the concentration profile becomes significantly more negative. A high Lewis number indicates stronger momentum diffusion relative to mass diffusion, which suppresses the mass transport. This results in sharper concentration gradients, causing a dip in concentration around the center of the parent branch.

5.2. Case 2: Daughter Artery

5.2.1. Daughter Velocity Profile

Figure 5(a): As the particle volume fraction increases, the daughter velocity shows a general increasing trend, possibly indicating a correlation between particle density and velocity, enhancing the interaction dynamics. Figure 5(b): A similar trend is noted where an increase in β results in higher daughter velocities, suggesting that thermal effects play a significant role in promoting the velocity dynamics. Figure 5(c): The daughter velocity demonstrates a pronounced increase with increasing Grashof number, supporting the hypothesis that buoyancy forces enhance the flow dynamics as thermal gradients increase. Figure 5(d): Increasing *Nb* again correlates positively with daughter velocity, indicating that buoyancy effects significantly contribute to fluid flow enhancement across the configuration. Figure 5(e): The relationship appears less pronounced than in previous subplots, indicating complex interactions between diffusion and convection processes affecting the daughter velocity. Figure 5(f): Variations in *Sr* show a significant effect on Vd, with higher values leading to increased velocities, potentially indicating that inertial forces become more influential at higher frequencies.

5.2.2. Daughter Temperature Profile

Figure 6(a): As ϕ increases, θd exhibits a gradual increase. Parameters involving ϕ likely influence the heat transfer characteristics in the system. Figure 6(b): Similar to subplot 6(a), higher values of β correlate with an increase in θd. This indicates that the thermal properties associated with β also adjust the temperature distribution. Figure 6(c): The family of curves shows a consistent trend of decreasing θd with higher *Nb*. Higher *Nb* values may suggest stronger influence of buoyancy, which could lead to reduced temperature. Figure 6(d): θd appears to rise with increasing *Le*, indicating more effective thermal diffusion. This suggests that as the thermal conductivity increases, the heat significantly spreads out across the domain. Figure 6(e): The trend indicates a decrease in θd with higher *Sr*. A larger *Sr* value implies a thicker boundary layer, which contributes to a lower overall temperature.

5.2.3. Daughter Concentration Profile

Figure 7(a): As ϕ increases, the Cd initially rises before sharply decreasing. This suggests that higher ϕ values influence peak concentrations as they transition towards a decline. Figure 7(b): The trend mirrors that of subgraph 7(a) where increasing β values lead to a pronounced decrease in Cd.

Parental Concentration

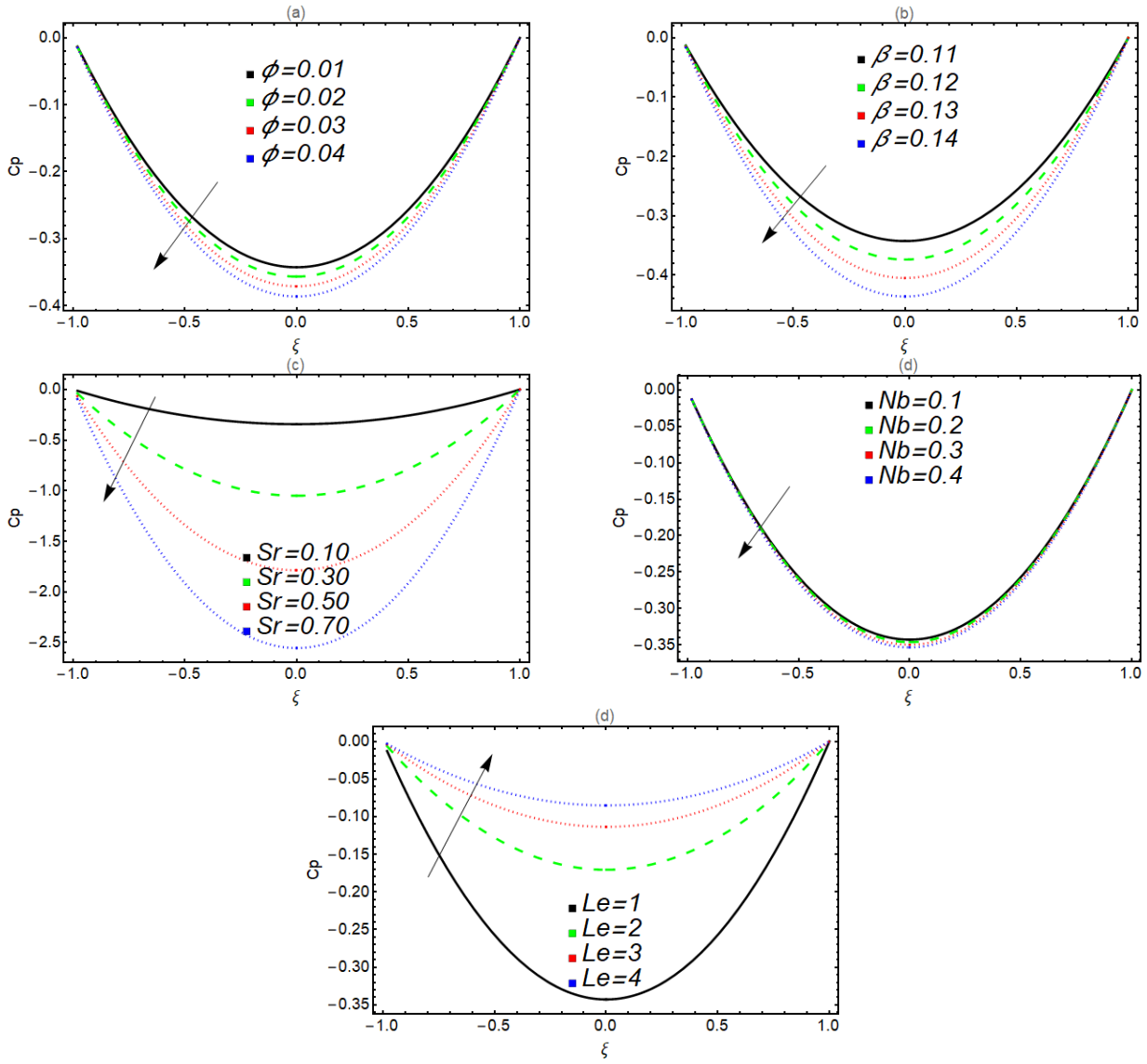

Figure 4: Parental Concentration Profile Cp on different variations of nanoparticle volume fraction ϕ, Brownian motion parameter *Nb*, Soret number *Sr*, and Lewis number *Le*, Thermal Expansion Coefficient β.

The variations indicate a critical threshold where the growth of Cd reverses. Figure 7(c): A clear trend showing that with increased *Nb*, the concentration of daughters also decreases. This may imply that greater *Nb* numbers correlate with lower concentration retention. Figure 7(d): Interestingly, as *Le* increases, the Cd fluctuates, indicating that the influence of thermal and mass diffusivity effects alters concentration dynamics distinctly, perhaps reflecting increasing stability in daughter concentration. Figure 7(e): An unexpected increase in Cd at lower *Sr* values indicates a complex relationship, where the *Sr* number evidently plays a critical role in altering oscillatory behavior affecting daughter concentrations.

Daughter Velocity

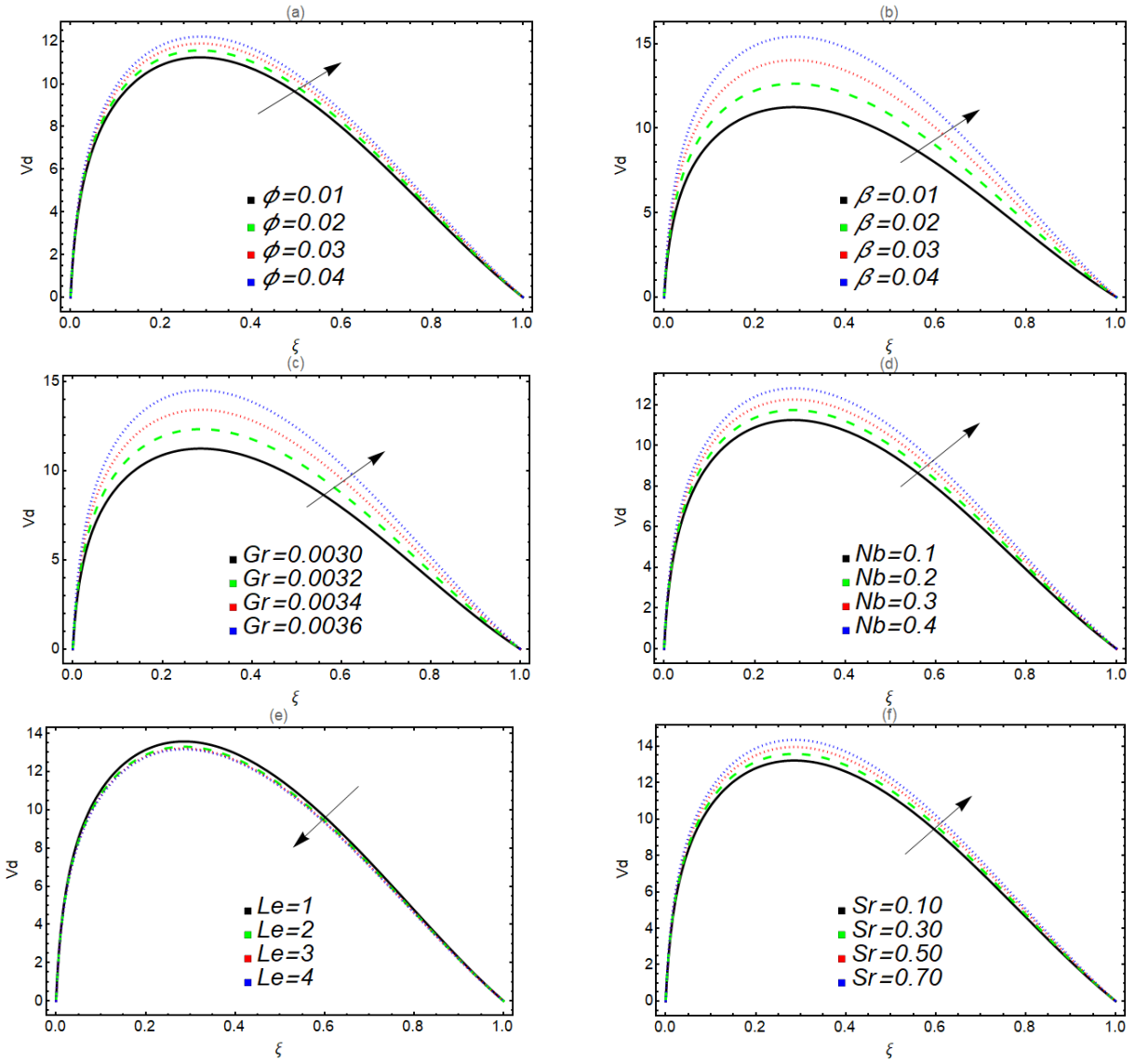

Figure 5: Daughter Velocity Profile *Vd* on different variations of nanoparticle volume fraction ϕ, Brownian motion parameter *Nb*, Soret number *Sr*, and Lewis number *Le*, Thermal Expansion Coefficient β, Grashof Number *Gr*.

6. Conclusions

6.1. Case 1: Parent Artery

In the parent artery region, the velocity, temperature, and concentration profiles demonstrate significant sensitivity to variations in nanofluid parameters. The velocity increases with higher nanoparticle volume fraction ϕ, thermal expansion coefficient β, Grashof number *Gr*, and Soret number *Sr*, indicating enhanced flow due to stronger thermal gradients and thermophoretic forces. The temperature distribution is elevated for increasing ϕ, β, and *Sr*, while Brownian motion *Nb* has a milder thermal influence. Concentration profiles tend to drop with increased ϕ, *Nb*, and *Sr* values, reflecting higher diffusion and nanoparticle dispersion. The Lewis number Le has the role of a damping term, which quells temperature as well as concentration distributions. All in all, the parent artery displays improved thermal and flow properties because of particle-induced effects essential in modelling behavior of flow around stenoses.

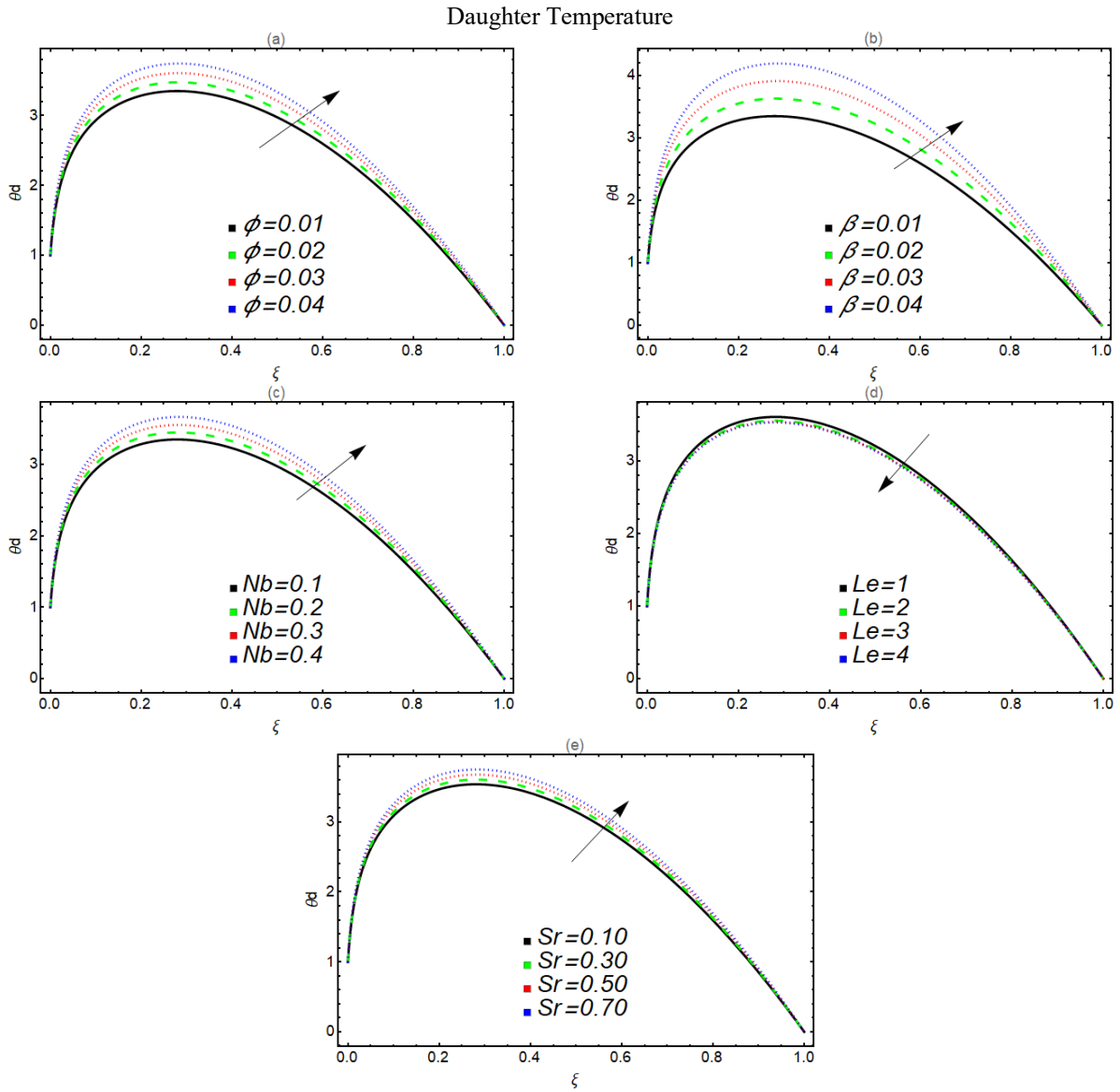

Figure 6: Daughter Temperature Profile θd on different variations of nanoparticle volume fraction ϕ, Brownian motion parameter *Nb*, Soret number *Sr*, and Lewis number *Le*, Thermal Expansion Coefficient β.

6.2. Case 2: Daughter Artery

In the daughter artery, thermal and velocity profiles indicate a synergistic interaction among thermophysical quantities. Velocity enhances with increasing ϕ, β, *Gr*, *Nb*, and *Sr*, complementing the effects of buoyancy and heat forces to enhance flow downstream. On the other hand, the temperature profile indicates distinct behavior, and though rising ϕ, β, and *Le* raise temperature, increased *Nb* and *Sr* lower it, suggesting opposing thermal transport processes. The concentration profile is non-monotonic; for example, ϕ and β increase concentration first before the drastic drop, and increased *Nb* and *Sr* result in lower concentrations. This is an indication that thermal and mass diffusion are differently behaved in diverging daughter branches. The region of the daughter artery thus proves that control of diffusivity plays a key role in nanoparticle delivery by targeted biomedical applications.

6.3. Overall Significance

The present study provides fundamental insight into the coupled heat–mass transport of nanofluids in stenosed bifurcated arteries. The newly developed concentration equation, incorporating curvature effects and branching flow dynamics, represents a significant advancement over conventional straight-channel models. Results demonstrate that careful tuning of nanoparticle volume fraction, Brownian motion

parameter, and Soret number can optimize both thermal management and targeted nanoparticle delivery in biomedical applications.

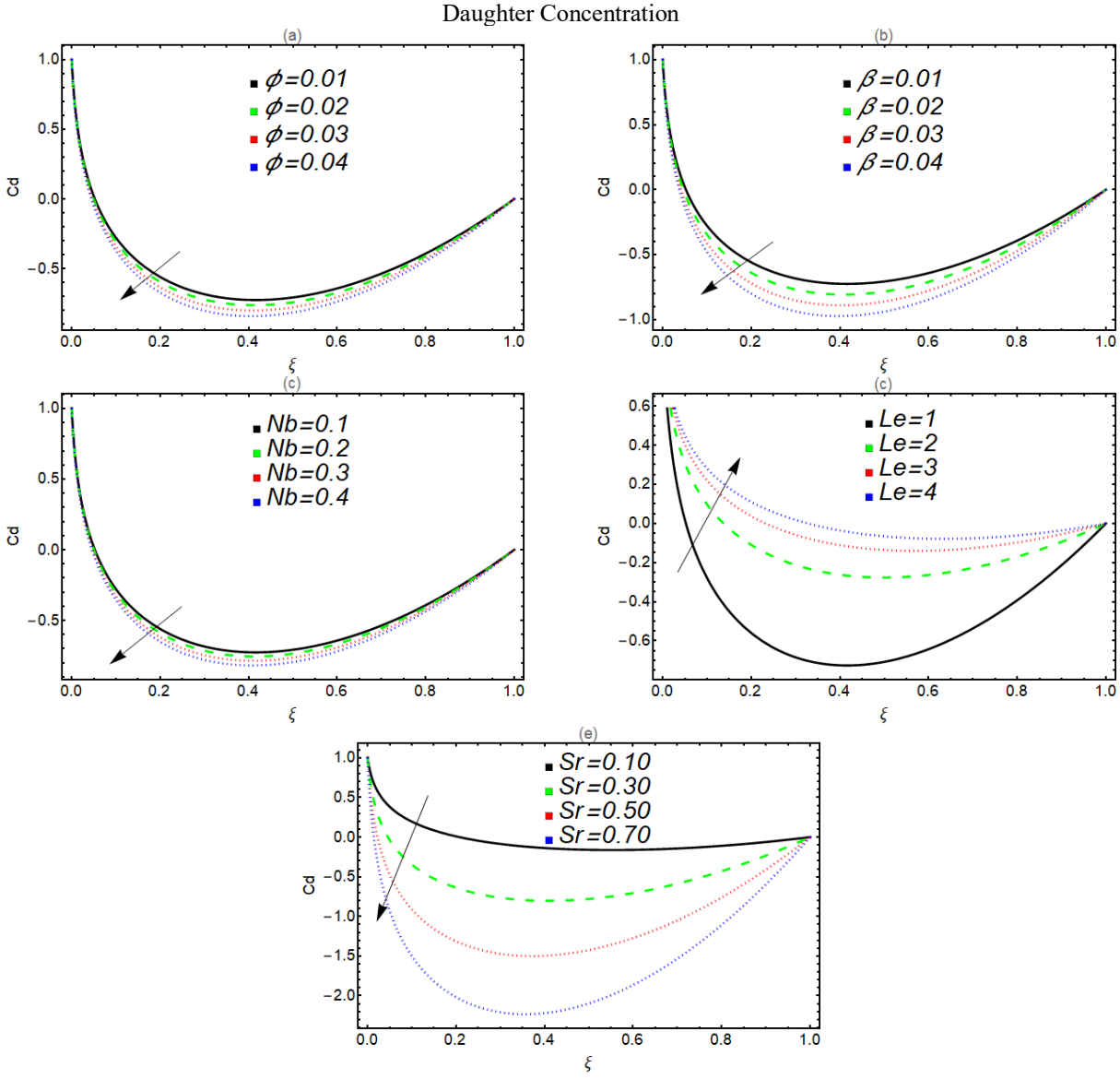

Figure 7: Daughet Concentration Profile Cd on different variations of nanoparticle volume fraction ϕ, Brownian motion parameter *Nb*, Soret number *Sr*, and Lewis number *Le*, Thermal Expansion Coefficient β.

Future work should extend this analysis to pulsatile flow regimes, include non-Newtonian blood rheology, and incorporate wall compliance effects to more accurately represent in vivo conditions. Additionally, experimental validation of the predicted concentration distributions would strengthen the clinical applicability of these theoretical findings.

Acknowledgements

The authors acknowledge the computational resources provided by International Islamic University Islamabad and COMSATS University Islamabad for the numerical analysis presented in this work.

References

[1] S. U. Choi, Enhancing thermal conductivity of fluids with nanoparticles, in *Proceeding of,* American Society of Mechanical Engineers, pp. 99-105.

[2] R. K. Tiwari, M. K. Das, Heat transfer augmentation in a two-sided lid-driven differentially heated square cavity utilizing nanofluids, *International Journal of heat and Mass transfer,* Vol. 50, No. 9-10, pp. 2002-2018, 2007.

[3] J. Buongiorno, Convective transport in nanofluids, 2006.

[4] R. Ellahi, S. Rahman, S. Nadeem, N. S. Akbar, Blood flow of nanofluid through an artery with composite stenosis and permeable walls, *Applied Nanoscience,* Vol. 4, No. 8, pp. 919-926, 2014.

[5] S. Nadeem, N. S. Akbar, Influence of heat and mass transfer on a peristaltic motion of a Jeffrey-six constant fluid in an annulus, *Heat and Mass transfer,* Vol. 46, No. 5, pp. 485-493, 2010.

[6] M. Sheikholeslami, M. Gorji-Bandpy, D. Ganji, Numerical investigation of MHD effects on Al2O3–water nanofluid flow and heat transfer in a semi-annulus enclosure using LBM, *Energy,* Vol. 60, pp. 501-510, 2013.

[7] M. Akbari, N. Galanis, A. Behzadmehr, Comparative analysis of single and two-phase models for CFD studies of nanofluid heat transfer, *International Journal of Thermal Sciences,* Vol. 50, No. 8, pp. 1343-1354, 2011.

[8] W. Khan, I. Pop, Boundary-layer flow of a nanofluid past a stretching sheet, *International journal of heat and mass transfer,* Vol. 53, No. 11-12, pp. 2477-2483, 2010.

[9] M. Rashidi, S. Abelman, N. F. Mehr, Entropy generation in steady MHD flow due to a rotating porous disk in a nanofluid, *International journal of Heat and Mass transfer,* Vol. 62, pp. 515-525, 2013.

[10] C. Caro, J. Fitz-Gerald, R. Schroter, Atheroma and arterial wall shear-observation, correlation and proposal of a shear dependent mass transfer mechanism for atherogenesis, *Proceedings of the Royal Society of London. Series B. Biological Sciences,* Vol. 177, No. 1046, pp. 109-133, 1971.

[11] D. N. Ku, D. P. Giddens, C. K. Zarins, S. Glagov, Pulsatile flow and atherosclerosis in the human carotid bifurcation. Positive correlation between plaque location and low oscillating shear stress, *Arteriosclerosis: An Official Journal of the American Heart Association, Inc.,* Vol. 5, No. 3, pp. 293-302, 1985.

[12] A. Quarteroni, M. Tuveri, A. Veneziani, Computational vascular fluid dynamics: problems, models and methods, *Computing and Visualization in Science,* Vol. 2, No. 4, pp. 163-197, 2000.

[13] C. A. Taylor, T. J. Hughes, C. K. Zarins, Finite element modeling of blood flow in arteries, *Computer methods in applied mechanics and engineering,* Vol. 158, No. 1-2, pp. 155-196, 1998.

[14] S. A. Ahmed, D. P. Giddens, Velocity measurements in steady flow through axisymmetric stenoses at moderate Reynolds numbers, *Journal of biomechanics,* Vol. 16, No. 7, pp. 505-516, 1983.

[15] C. M. Spaegele, 2024, *Controlling Photons, Electrons, and Polaritons at the Nanoscale—Towards the Next Generation of Optoelectronic Devices*, Harvard University,

[16] K. Perktold, G. Rappitsch, Computer simulation of local blood flow and vessel mechanics in a compliant carotid artery bifurcation model, *Journal of biomechanics,* Vol. 28, No. 7, pp. 845-856, 1995.

[17] A. Valencia, F. Baeza, Numerical simulation of fluid–structure interaction in stenotic arteries considering two layer nonlinear anisotropic structural model, *International Communications in Heat and Mass Transfer,* Vol. 36, No. 2, pp. 137-142, 2009.

[18] F. Mebarek-Oudina, Convective heat transfer of Titania nanofluids of different base fluids in cylindrical annulus with discrete heat source, *Heat Transfer—Asian Research,* Vol. 48, No. 1, pp. 135-147, 2019.

[19] M. Bhatti, A. Zeeshan, R. Ellahi, N. Ijaz, Heat and mass transfer of two-phase flow with Electric double layer effects induced due to peristaltic propulsion in the presence of transverse magnetic field, *Journal of Molecular Liquids,* Vol. 230, pp. 237-246, 2017.

[20] O. U. Mehmood, S. Bibi, A. Zeeshan, M. M. Maskeen, F. Alzahrani, Electroosmotic impacts on hybrid antimicrobial blood stream through catheterized stenotic aneurysmal artery, *The European Physical Journal Plus,* Vol. 137, No. 5, pp. 585, 2022.